VOL. 7, NO. 8, AUGUST 2012 ISSN 1819-6608
ARPN Journal of Engineering and Applied Sciences


www.arpnjournals.com

INVESTIGATION THE DYNAMIC STRESSES OF VIBRATION IN OUTER RACE OF LOW SPEED BALL BEARING

Thaker Salih Dawood
Faculty of Agriculture and Forestry, University of Duhok, Duhok, Iraq
E-Mail: Thakr1960@yahoo.com

ABSTRACT

The race ring in vehicle are subjected to sever load acting between the rolling elements and raceways in rolling bearings which develop only small area of contact between the mating members. Large level of stresses is developed on the surface of the rolling elements and raceways. Consequently, although the elemental loading may only be moderate, stresses induced on the surfaces of the rolling elements and raceways are usually large. The determination of deformation and stress distributions due to both static and dynamic loading is essential in the design stage of the raceways. Finite element model of a stress analysis of the ball bearing has been built considering the race ring as a plane stress problem and choosing the 8 = node isentropic quadrilateral element. A computer package Ansys/5.4 for both static and dynamic analysis. The more damping ratio used, the more stabilizing of the stresses with respect to time.

Keywords: ball bearing analysis, finite element method, stress analysis methods.

INTRODUCTION

Ball and roller bearings are commonly used in machine element. They are employed to permit rotary motion of or about shafts in simple commercial devices as bicycles, roller shaft, and electric motors. They are also utilized in complex engineering mechanisms including among many others, aircraft gas turbine, rolling mills, dental drill assembles, gyroscope, and power transmission. Usually a bearing may obtained as a unit, which include two steel rings each of which has a hardened raceway in which hardened steel balls or rollers roll. The race is a thin shell of revolution, which received its loading from the balls surrounding the shell through the contact, occurred between them (the race and the balls) due to loading.

Gustafson *et al*. (1963) studied the effects of waviness and pointed out that lower order ring waviness affects the amplitude of the vibrations at the ball passage frequency. They observed that vibrations at higher harmonics of the ball passage frequency are also present in the vibration spectrum and their amplitudes depend on the radial load, radial clearance, rotational speed and the order of harmonics [1]. The same conclusion was theoretically proved by Meyer *et al*. (1980) for perfect radial ball bearings with linear modeling of the spring characteristics of balls [2]. Gad *et al*. (1984) showed that resonance occurs when BPF coincides with the frequency of the system and they also pointed out that for certain speeds, BPF can exhibit its sub and super harmonic vibrations for shaft ball bearing systems [3]. Ji-Huan He (2000) developed some analytical techniques for solving nonlinear equations. These techniques are used to increase numerical stability and decrease the computer time for system analysis [4].

El-Sayed (1980) derived a form of equation for the stiffness of bearings and determined total deflections of inner and outer races caused by an applied load, using the Hertz theory [5]. Tamura and Tsuda (1980) performed a theoretical study of fluctuations of the radial spring characteristics of a ball bearing due to ball revolutions [6]. Wardle and Poon (1983) pointed out the relations between the number of balls and waves for sever vibrations to occur. When the number of balls and waves are equal there would be severing vibrations [7]. Wardle (1988a) showed that ball waviness produced vibrations in the axial and radial directions at different frequencies and also pointed out that only even orders of ball waviness produced vibrations [8].

Loading mechanism

The loads applied to rolling bearings are transmitted through the rolling elements from the inner ring to the outer ring. The magnitude of the loading carried by the individual ball or roller depends on the internal geometry of the bearing and the type of load applied to it.

In most bearing applications, only applied radial, axial, or a combination of radial and axial loadings are considered. However, under very heavy applied loading or if shafting is hollow, the shaft where the bearing is mounted may bend, causing a significant moment load on the bearing. Also, the bearing housing may be non rigid due to design targeted at minimizing both size and weight, causing it to bend while accommodating moment loading. This combined radial, axial, and moment loadings result in distorted distribution of load among the bearing's rolling element complement. This may cause significant changes in bearing deflections, contact stresses, and fatigue endurance compared to the operating parameters which have the simpler load distributions. To simplify the analytical process, load applied is assumed pure radial load in this study. The load distribution around the circumference of a rolling element bearing under radial load (as shown in Figure-1) is defined approximately by the Stribeck equation [10]:

$$q(\psi) = q_0 [1 - \frac{1}{2\varepsilon}(1 - \cos\psi)]^n \quad (1)$$

Where q_0 is the maximum load intensity at $\psi = 0^0$, ε is the load distribution factor and n denotes the load deflection exponent. For ball bearing n is 1.5 while for roller bearing n is 1.11.

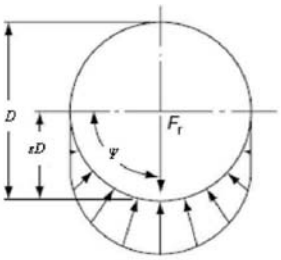

Figure-1. The load distribution in a bearing under radial load.

The maximum load intensity, q_0, for ball bearing having zero clearance and subjected to a simple radial load can be approximated by,

$$q_0 = \frac{4.37F_r}{Z\cos\alpha} \quad (2)$$

Where F_r is the radial load and Z is the number of balls and α is contact angle.
The load distribution factor, ε, is defined by,

$$\varepsilon = \frac{1}{2}(1 - \frac{p_d}{2\delta_r}) \quad (3)$$

Where P_d denotes the diameter clearance, while δ_r is the ring radial shift. If the diameter clearance is assumed as 0, hence the value of ε is 0.5.

The rolling elements transfer the radial load to the outer ring during their rotation with the cage frequency, f_c, expressed as:

$$f_c = \frac{f_s}{2}(1 - \frac{d_d}{d_m}\cos\alpha) \quad (4)$$

Where, f_s is the shaft frequency, d_b and d_m is ball diameter and pitch diameter, respectively. Since in this study assumed that the ball bearing is subjected to a pure radial load, hence the contact angle will be 0^0.

Modeling of the system

As a first step in investigating the vibrations characteristics of ball bearings, a model of a rotor-bearing assembly can be considered as a spring-mass system, where the rotor acts as a mass and the raceways and balls act as mass less nonlinear contact springs. In the model, the outer race of the bearing is fixed in a rigid support and the inner race is fixed rigidly with the rotor. A constant radial vertical force acts on the bearing. Therefore, the system undergoes nonlinear vibrations under dynamic conditions.

Elastic deformation between the race and ball gives a non-linear force deformation relation, which is obtained by using the Hertzian theory. Other sources of stiffness variation are the positive internal radial clearance, the finite number of balls whose position changes periodically and waviness at the inner and outer race. They cause periodic changes in stiffness of the bearing assembly. Taking into account these sources of stiffness variation the governing differential equations are obtained.

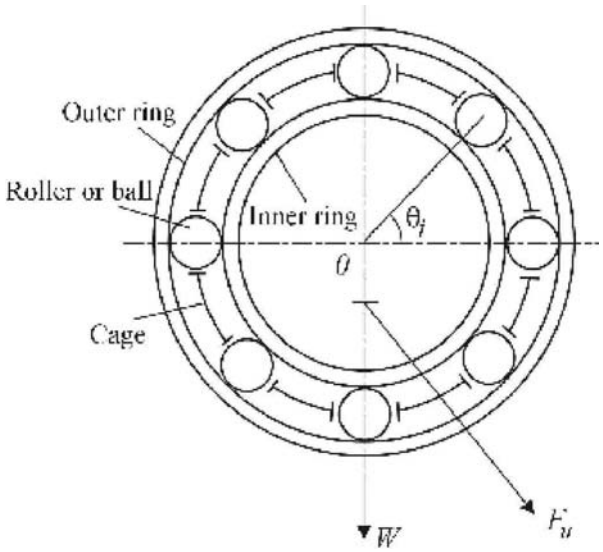

Figure-2. A schematic diagram of a rolling element bearing.

A schematic diagram of a rolling element bearing is shown in Figure-1. In the mathematical model, the ball bearings are considered as a non-linear mass-spring system. Since the Hertzian forces arise only when there is contact deformation, the springs are required to act only in compression. In other words, the respective spring force comes into play when the instantaneous spring length is shorter than its unstressed length, otherwise the separation between the ball and race takes place and the resulting force is set to zero. An unbalance force (Fu) is due to rotating of the shaft with inner race. The assumptions made in the development of the mathematical model are as follows:

a) Balls are positioned equi-pitched around the inner race and there is no interaction between them.
b) The outer race is fixed rigidly to the support and the inner race is fixed rigidly to the shaft.
c) The ball, inner and outer races and the cage have motions in the plane of the bearing only. This eliminates any motion in the axial direction.
d) The bearings are assumed to operate under isothermal conditions.
e) There is no slipping of balls as they roll on the surface of races.

f) The races are flexural rigid and undergo only local deformations due to the stresses in contacts,
g) Deformations occur according to the Hertzian theory of elasticity.

Contact stiffness

Hertz considered the stress and deformation in the perfectly smooth, ellipsoidal, contacting elastic solids. The application of the classical theory of elasticity to the problem forms the basis of stress calculation for machine elements such as the ball and roller bearings. Therefore the point of contact between the race and ball develops into a contact area which has the shape of an ellipse with *a* and *b* as the semi major and semi minor axes respectively. The curvature sum and difference are needed in order to obtain the contact force of the ball. The curvature sum $\sum\rho$ obtained following Harris (1991) is expressed as:

$$\sum\rho = \rho_{11} + \rho_{12} + \rho_{11\,1} + \rho_{11\,2} = \frac{1}{r_{11}} + \frac{1}{r_{12}} + \frac{1}{r_{11\,1}} + \frac{1}{r_{11\,2}} \quad (5)$$

The curvature difference $F(\rho)$ is expressed as:

$$F(\rho) = \frac{(\rho_{11} - \rho_{12}) + (\rho_{11\,1} - \rho_{11\,2})}{\sum\rho} \quad (6)$$

The parameters r_{11}, r_{12}, $r_{11\,1}$, $r_{11\,2}$ ρ_{11}, ρ_{12} , $\rho_{11\,1}$,$\rho_{11\,2}$ are given dependent upon calculations referring to the inner and outer races as shown in Figure-3.

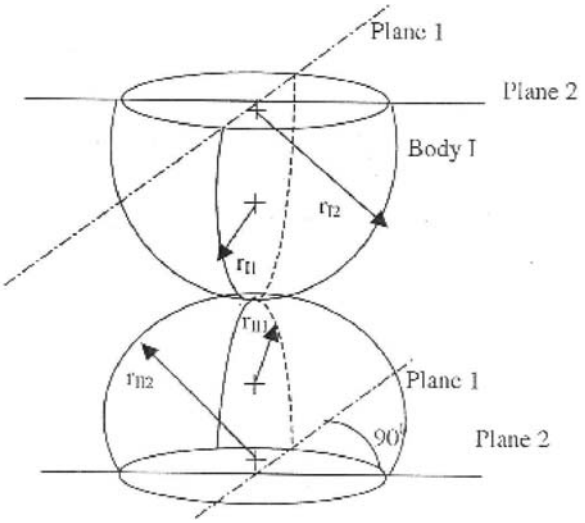

Figure-3. Geometry of contacting bodies.

If the inner race is considered

r_{11} = D/2, r_{12} = D/2, $r_{11\,1}$ = d_1/2, $r_{11\,2}$ = r_1 and (7)

ρ_{11} = 2/D, ρ_{12} = 2/D, $\rho_{11\,1}$ = 2/d_1, $\rho_{11\,2}$ = -1/r_1

If the outer race is considered, they are given as:

r_{11} = D/2, r_{12} = D/2, $r_{11\,1}$ = d_0/2, $r_{11\,2}$ = r_0 and (8)

ρ_{11} = 2/D, ρ_{12} = 2/D, $\rho_{11\,1}$ = -2/d_0, $\rho_{11\,2}$ = -1/r_0

As per the sign convention followed, negative radius denotes a concave surface. Using Table-2, we can calculate all the parameters including the curvature difference at the inner and outer race. For the contacting bodies made of steel, the relative approach between two contacting and deforming surfaces is given by:

$$\delta = 20787x10^{-8} Q^{2/3} (\sum\rho)^{1/3} \delta^* \quad (9)$$

where δ^* is a function of *F(p)*.
Hence, the contact force *(Q)* is

$$Q = \left\{3.587\times10^{7} \left(\sum\rho\right)^{1/2} \left(\delta^*\right)^{-3/2}\right\} \delta^{3/2} \quad (N) \quad (10)$$

The elastic modulus for the contact of a ball with the inner race is

$$\left[K_1 = 3.587\times10^{7} \left(\sum\rho\right)^{-1/2} \left(\delta_1^*\right)^{-3/2} \quad \left(\frac{N}{mm}\right)\right] \quad (11)$$

And for the contact of a ball with the outer race is

$$K_0 = 3.587\times10^{7} \left(\sum\rho_0\right)^{-1/2} \left(\delta_0^*\right)^{-3/2} \quad \left(\frac{N}{mm}\right) \quad (12)$$

Then the effective elastic modulus *K* for the bearing system is written as:

$$K = \frac{1}{\left(1/K_1^{1/n} + 1/K_0^{1/n}\right)^n} \quad (13)$$

In Eqs (11) and (12), the parameters δ^* and δ^* can be obtained from Table-1, where as the values of $F(p)_1$ and $F(p)_0$ are available from Table-2. The effective elastic modulus *(K)* for a bearing system using geometrical and physical parameters is written as:

$$K = 7.055\times10^{5}\sqrt{\delta} \quad \left(\frac{N}{mm}\right) \quad (14)$$

Table-1. Dimensional contact parameters by harris (1991) [10].

F(P)	δ*
0	1
0.1075	0.997
0.3204	0.9761
0.4795	0.9429
0.5916	0.9077
0.6716	0.8733
0 7332	0.8394
0 7948	0 7961
0.83595	0 7602
0.87366	0.7169
0.90999	0.6636
0.93657	0.6112
0.95738	0.5551
0.97290	0.4960
0.983797	0.4352
0.990902	0.3745
0.995112	0.3176
0.997300	0.2705
0.9981847	0.2427
0.9989156	0.2106
0.9994785	0.17167
0.9998527	0.11995
1	0

Table-2. Geometric and physical properties used for the ball bearings.

Ball radius (r_b)	6mm
Inner race radius (r_i)	23mm
Outer race radius (r_o)	46mm
Internal radial clearance (g)	0.1 µm
Radial load (W)	5900N
Mass of bearing (m)	0.6 kg
Modulus of elasticity	200000 MPa
Number of balls (N_b)	9
Inner race groove radius (r_{gi})	4.08mm
Outer race groove radius (r_{go})	4.61mm
Speed of the rotor (N_r)	500rpm
Pitch radius of the ball set (r_m)	27mm

RESULTS AND DISCUSSIONS

Its important to show that the indicated numbers (1, 2, 3, 4, 5, 6, 7, 8, 9, 10, 11, 12, 13, 14, 15, 16, 17) from figures (6, 7, 8, 9, 10) denoted to the nodes (188, 189, 190, 191, 192, 193, 194, 195, 196, 197, 198, 199, 200, 201, 202, 203, 204), and from figures (11, 12, 13, 14, 15) denoted to the nodes (167, 216, 260, 241, 195, 142, 80, 53, 312, 294) respectively, as shown in Figure-4.

Figures 6 and 7 show the values of Ux and Uz displacement along the surface of longitudinal line of outer race way groove. It is seems that the maximum displacements (Ux = -0.005mm, Uz = -0.005mm) occur between nodes (4 and 6) which represents the contact area between the ball and the outer race way. The minus sign indicates to the direction of the deformation occur to the race way. Figure-8 shows the comparison between the behavior of Ux and Uz displacements in case of the longitudinal line of action, it's obvious that the same behavior can be obtained.

Figure-9 shows the deformation in (xz direction), the maximum deformation (Uxz = -0.005mm) and it's approximate between node (4 and 6).

Figure-10 indicates the von misses stresses for the longitudinal line nodes, the maximum von misses stresses (32 Mpa) is located in node (4) which is the location of the maximum loading inside the contact area between the ball and the outer raceway.

Figures 11 and 12 shows the Ux and Uz displacements along the lateral line, similar behaviors can be obtained to that the longitudinal line, the maximum displacement (Ux = -0.0048 mm, Uz = -0.005 mm) occur between nodes (8) and node (9), also in these results the minus sign indicates the direction of the displacements occur in the lateral line.

Figure-13 shows the comparison between the behavior of Ux and Uz values of displacements in case of the lateral line of action.

Figure-14 shows the comparison between the behavior of Ux and Uz displacements in case of the lateral line of action, it's obvious that the same behavior can be obtained.

The von misses stresses was presented in Figure-15 for the lateral line nodes, in this figure it clear that the maximum von misses stresses is (30 Mpa) occur between nodes (8) and (9).

Comparing between Figures 10 and 15, it's clear that in Figure-10 the maximum von misses stresses was located in node (4), while in Figure-15 the maximum von misses stresses enclosed between nodes (8) and (10).

For the dynamic results obtained the Figures 16 and 17 shows the dynamic behavior of Ux and Uz with time during damping ratio (0.04) along the longitudinal line of action. Figure-18 clears the von misses' dynamic behavior with time during damping (0.04) along the longitudinal line of action. In Figures 19 and 20, the dynamic behavior of (Ux) and (Uz) was expressed with time using damping ratio (0.05). The dynamic behavior of von misses stresses with time using damping ratio (0.05) was obvious in Figure-21. When damping ratio (0.06) was

used, the dynamic behavior with time of Ux and Uz was represented in Figures 22 and 23. Figure-24 shows the behavior of von misses stresses with time using damping ratio (0.06). The time of dynamic simultaneous was (5) seconds and the sub step equal to (10) sub step each sub step equal (0.5) second.

CONCLUSIONS

The model analysis of the ball bearing that was used in this paper considers elastic characteristics and the obtained results express the behavior of deformation, and stresses with different conditions for the deformation along x-axis, it can be concluded the same behavior can be obtained for the two conditions (longitudinal and lateral) due to the direction of the applied force acting between the outer race and the ball. Also for deformation along xz-axis, the same behavior has been obtained with minus sign indicates the total direction of deformed race. The location of the maximum deformations for both Ux and Uz was congruency with the mathematical model calculations, with represent to the area of contact between the ball and outer race.

Von misses' stresses behavior was similar to both cases (longitudinal and lateral). Also there was congruency between the numerical and mathematical work for the location of maximum von misses stresses. For dynamic analysis, it was clear that the work damping ratio used, the more stabilizing in the stresses and deformation with respect to time.

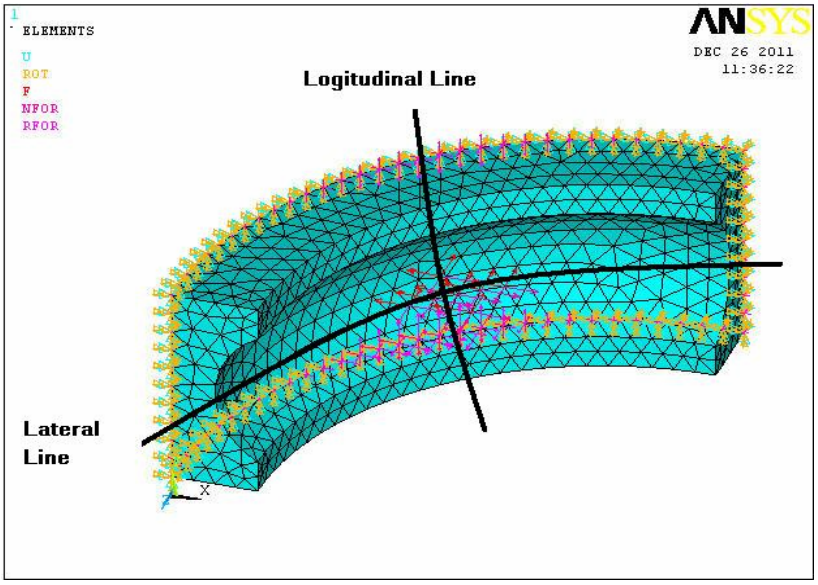

Figure-4. Geometry of outer race section.

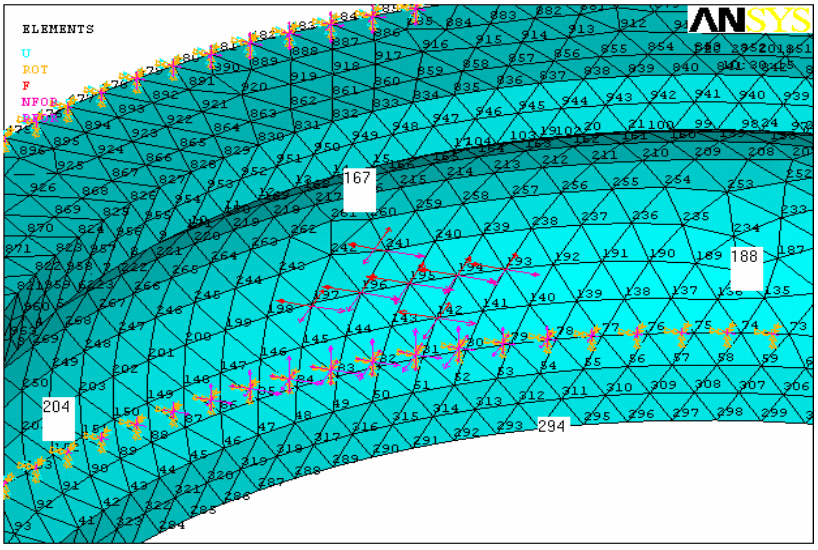

Figure-5. Nodes along line of load effect and surface of raceway groove.

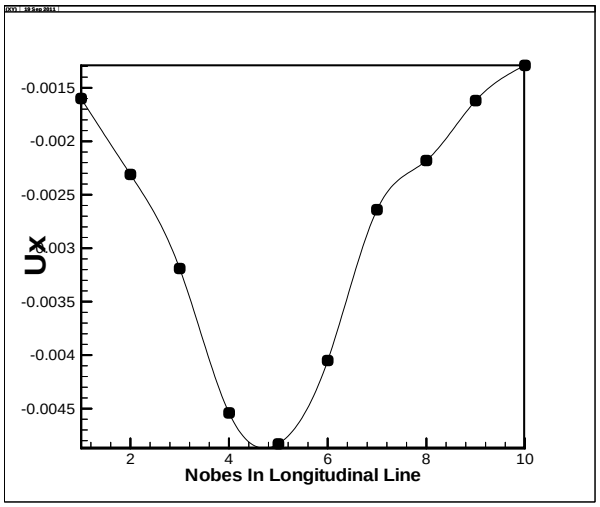

Figure-6. Deformation in x-direction.

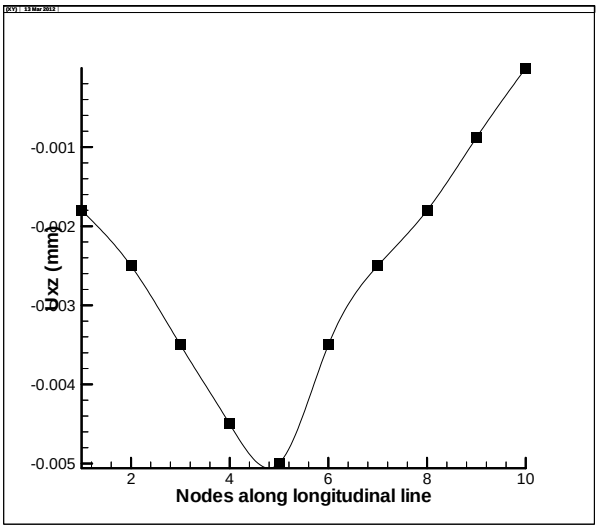

Figure-9. Deformation in xz-direction.

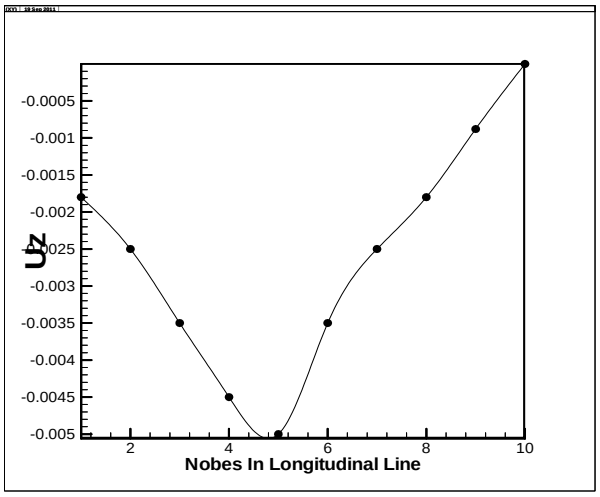

Figure-7. Deformation in z-direction.

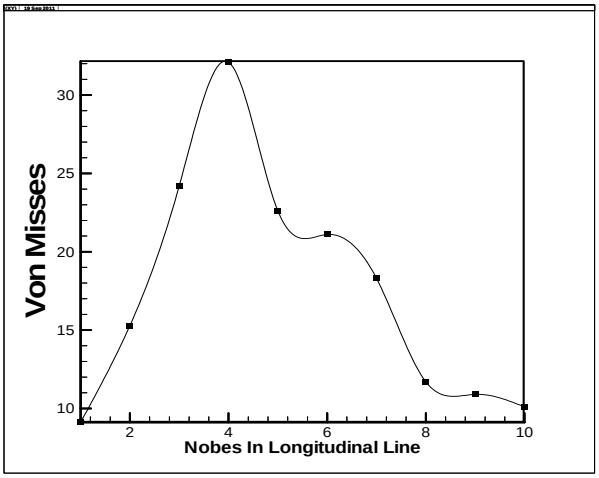

Figure-10. Von Misses in longitudinal line.

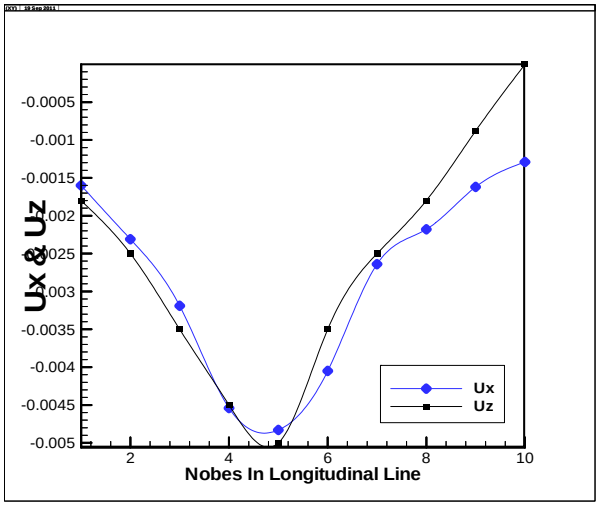

Figure-8. Comparison deformation in (x and z)-direction.

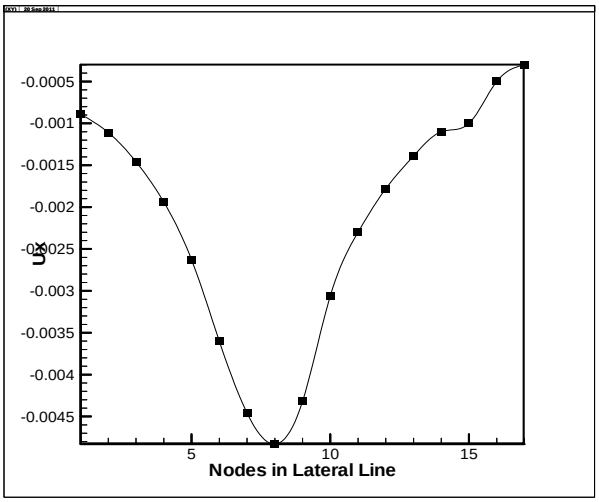

Figure-11. Deformation in x-direction.

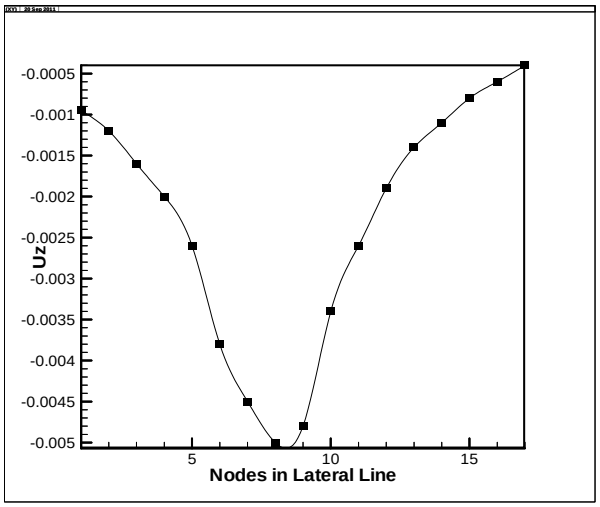

Figure-12. Deformation in z-direction.

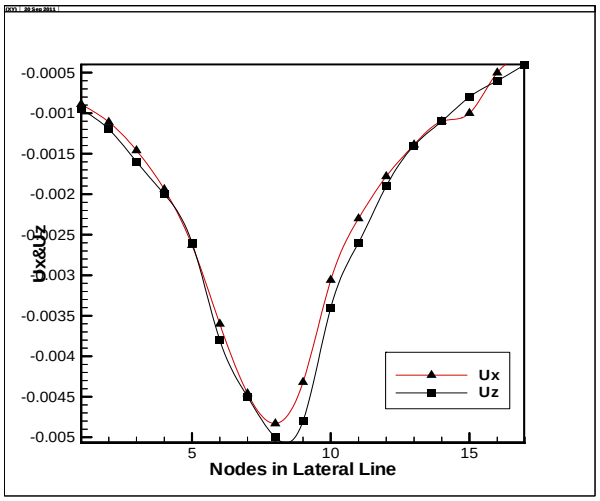

Figure-13. Comparison deformation in (x and z) direction.

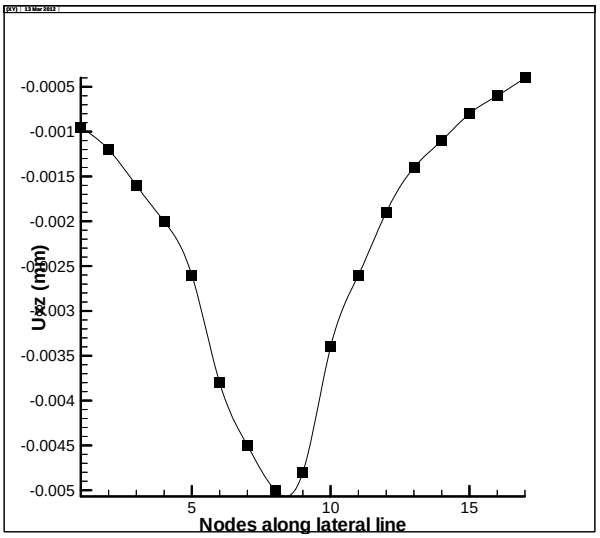

Figure-14. Deformation in (x and z) direction.

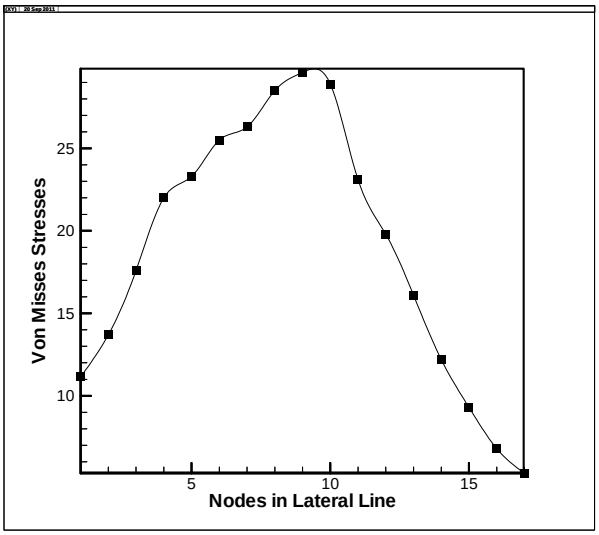

Figure-15. Von misses in lateral line.

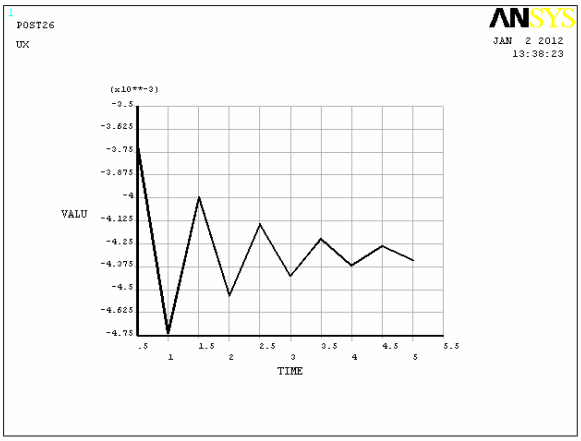

Figure-16. Dynamic stress of Ux when damping coefficient = 0.04.

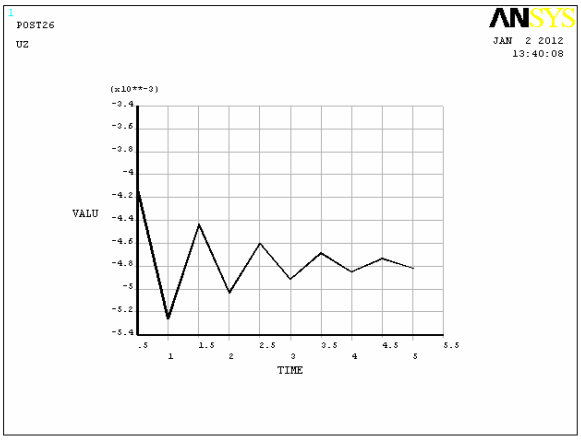

Figure-17. Dynamic stress of Uz when damping coefficient = 0.04.

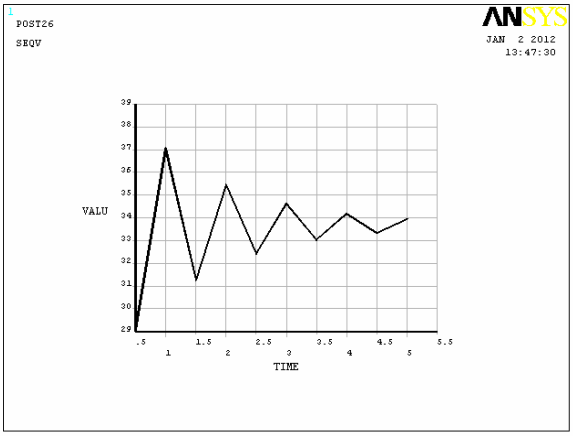

Figure-18. Dynamic stress of Von misses when damping coefficient = 0.04.

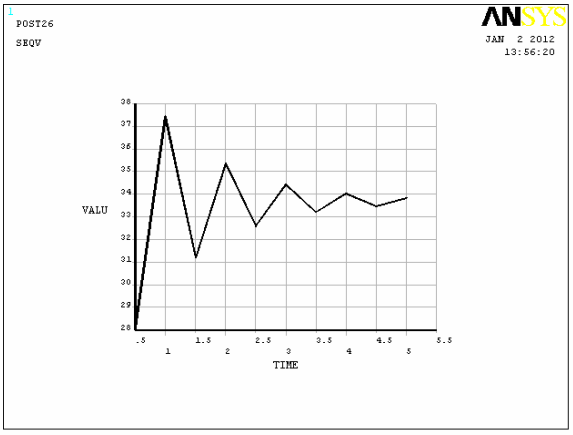

Figure-21. Dynamic stress of Von misses when damping coefficient = 0.05.

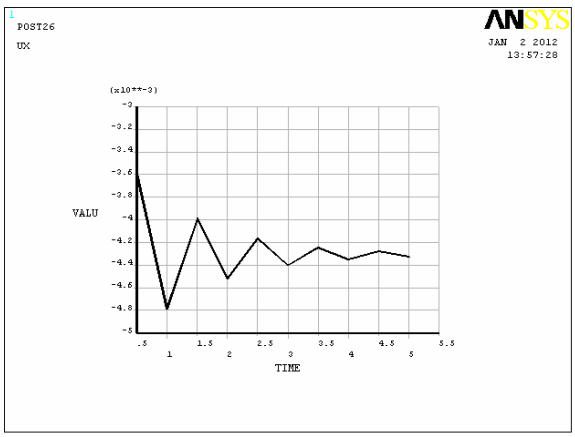

Figure-19. Dynamic stress of Ux when damping coefficient = 0.05.

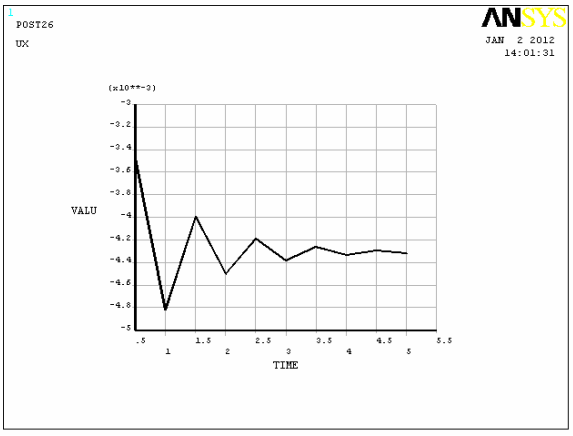

Figure-22. Dynamic stress of Ux when damping coefficient = 0.06.

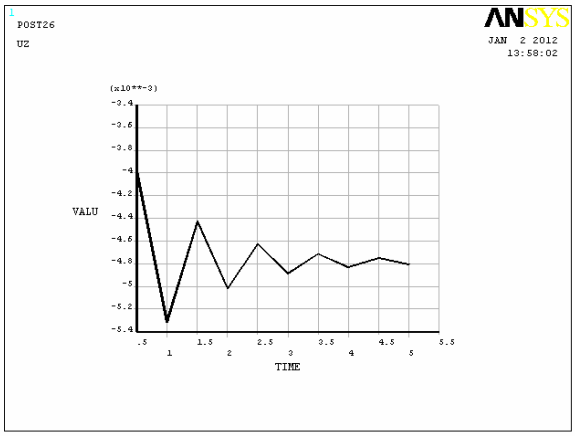

Figure-20. Dynamic stress of Uz when damping coefficient = 0.05.

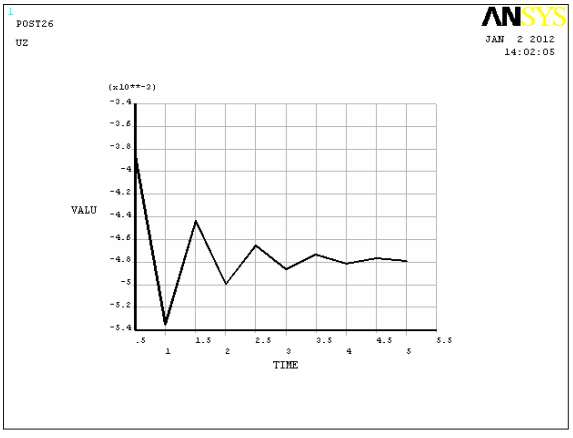

Figure-23. Dynamic stress of Uz when damping coefficient = 0.06.

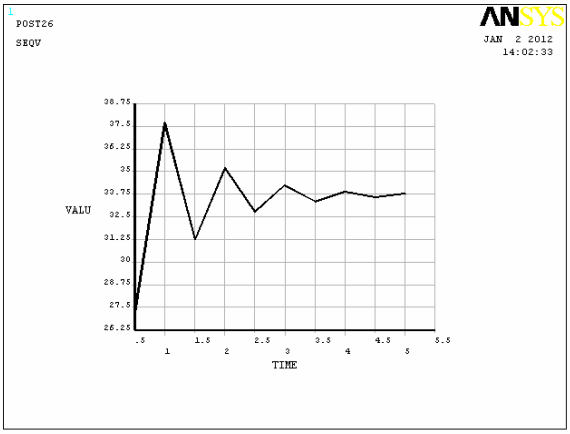

Figure-24. Dynamic stress of Von misses when damping coefficient = 0.06.

REFERENCES

[1] Gustafson O.G. and Tallian T. *et al*. 1963. Research Report on study of the Vibration Characteristics of Bearings. Reg: 585 14: 4223, Dec. Report: A L 631 023, SKF Ind. Inc.

[2] Meyer L.D., Ahlgran F.F. and Weichbrodt B. 1980. An analytical model for ball bearing vibrations to predict vibration response to distributed defects. ASME Journal of Mechanical Design. 102: 205-210.

[3] Gad E.H., Fukata S. and Tamura H. 1984. Computer simulation of rotor axial and radial vibrations due to ball bearings. Memories of the Faculty of Engineering, Kyushu University. 44: 169-189.

[4] He J.H. 2000. A review on some new recently developed nonlinear analytical technique. Int. Journal Nonlinear Sciences and Numerical Simulation. 1: 51-70.

[5] El-Sayed H.R. 1980. Stiffness of deep-groove ball bearings. Wear. 63: 89-94.

[6] Tamura H. and Tsuda Y. 1980. On the spring characteristics of ball bearing (Extreme characteristics with many balls). Bulletin of JSME. 23: 961 -969.

[7] Wardle F.P. and Poon S.Y. 1983. Rolling bearing noise, cause and cure. Char. Mechanical Engineering. July/Aug. pp. 36-40.

[8] Wardle F.P. 1988a. Vibration forces produced by waviness of the rolling surfaces of thrust loaded ball bearings. Part I: Theory. Proc. JJVIechE. 202 (C5): 305-312.

[9] Aktiirk N. 1999. The effect of waviness on vibrations associated with ball bearings. ASME Journal of Tribology. 121: 667-677.

[10] Harris T.A. 1991. Rolling Bearing Analysis. New York: Willey, USA.